8528 *Biochemistry* **2009,** *48,* 8528–8539
DOI: 10.1021/bi900616w

BIOCHEMISTRY
including biophysical chemistry & molecular biology
Article

The Cytosolic Half of Helix III Forms the Substrate Exit Route during Permeation Events of the Sodium/Bile Acid Cotransporter ASBT†

Naissan Hussainzada, Tatiana Claro Da Silva, and Peter W. Swaan*

Department of Pharmaceutical Sciences, University of Maryland, Baltimore, Maryland 21201

Received April 9, 2009; Revised Manuscript Received July 8, 2009

ABSTRACT: Site-directed alkylation of consecutively introduced cysteines was employed to probe the solvent-accessible profile of highly conserved transmembrane helix 3 (TM3), spanning residues V127−T149 of the apical sodium-dependent bile acid transporter (ASBT), a key membrane protein involved in cholesterol homeostasis. Sequence alignment of SLC10 family members has previously identified a signature motif (ALGMMPL) localized to TM3 of ASBT with as yet undetermined function. Cysteine mutagenesis of this motif resulted in severe decreases in uptake activity only for mutants M141C and P142C. Additional conservative and nonconservative replacement of P142 suggests its structural and functional importance during the ASBT transport cycle. Significant decreases in transport activity were also observed for three cysteine mutants clustered along the exofacial half of the helix (M129C, T130C, S133C) and five mutants consecutively lining the cytosolic half of TM3 (L145C−T149C). Measurable surface expression was detected for all TM3 mutants. Using physicochemically different alkylating reagents, sites predominantly lining the cytosolic half of the TM3 helix were found to be solvent accessible (i.e., S128C, L143C−T149C). Analysis of substrate kinetics for select TM3 mutants demonstrates significant loss of taurocholic acid affinity for mutants S128C and L145C−T149C. Overall, we conclude (i) the functional and structural importance of P142 during the transport cycle and (ii) the presence of a large hydrophilic cleft region lining the cytosolic half of TM3 that may form portions of the substrate exit route during permeation. Our studies provide unique insight into molecular mechanisms guiding the ASBT transport cycle with respect to substrate binding and translocation events.

Efficient recirculation of the body's bile acid pool proceeds via multiple active and passive transport routes lining the enterohepatic pathway. Along the distal ileum, the apical sodium/bile acid cotransporter ASBT (SLC10A2) constitutes the chief mechanism for reclaiming bile acids secreted into the gut in response to food intake (*1*). Functioning as a sodium symporter, the relatively small ASBT protein (348 amino acids, 41 kDa) transduces the free energy stored in electrochemical ion gradients into solute concentration gradients, resulting in the translocation of one bile acid molecule per (approximately) two sodium ions per transport cycle (*2*). As bile acids are the catabolic product of cholesterol metabolism, ASBT also plays a physiologically critical role in cholesterol homeostasis (*3*). Pharmaceutically, the intimate link between cholesterol and ASBT can be exploited to generate therapeutics aimed at hypercholesterolemia indications (*4*−*10*) and prodrug approaches to increase oral bioavailability (*11*, *12*).

Previous work from our laboratory has confirmed a seven-transmembrane (7TM)[1] spanning topology for ASBT (*13*, *14*) from which an *in silico* homology model was generated (*14*). Since these initial studies, we have employed a combination of biochemical and *in silico* approaches to identify protein components mediating substrate recognition and binding (*15*−*18*) in an attempt to unravel individual mechanistic steps of the ASBT transport cycle (*19*). These previous studies relied on experimental schemes that exploited the affinity of thiol groups on consecutively introduced cysteine residues to chemical modification by methanethiosulfonate (MTS) reagents (Figure 1A). Since reactivity (i.e., accessibility) of an introduced thiol depends on its local protein environment and can be severely limited by the low dielectric constants found within lipid or internal protein surroundings, this protocol can resolve the solvent-accessible profile of integral membrane proteins. Moreover, any alterations in the surrounding protein environment in response to substrate binding can manifest as changes in reactivity of the introduced thiol to various alkylating probes. Therefore, a dynamic impression of the global changes in protein structure occurring during the transport cycle may be gleaned from these studies, thus offering novel insight into mechanistic details of solute transport (*20*).

Here, we investigate the role of the highly conserved transmembrane helix 3 (TM3) using site-directed alkylation techniques. TM3 mutants were constructed against the C270A parental template, since native ASBT protein contains endogenous cysteines that are susceptible to thiol modification. Use of the C270A template circumvents thiol reactivity issues inherent to the native protein, since C270A displays minimal thiol reactivity and constitutes the only endogenous cysteine available for modification via biotin-linked thiol reagents. Using the C270A template, positions V127−T149 were individually replaced with cysteine and probed with MTS reagents based on the following

†This work was supported by National Institutes of Health Grant DK061425.

*To whom correspondence should be addressed. Tel: 410-706-7059. Fax: 410-706-7059. E-mail: pswaan@rx.umaryland.edu.

[1]Abbreviations: EL, extracellular loop; hASBT, human apical sodium-dependent bile acid transporter; MTS, methanethiosulfonate; MTSEA-biotin, (2-((biotinoyl)amino)ethyl methanethiosulfonate); MTSET, [2-(trimethylammonium)ethyl] methanethiosulfonate bromide; SCAM, substituted cysteine accessibility method; TM, transmembrane.

 Published on Web 08/04/2009

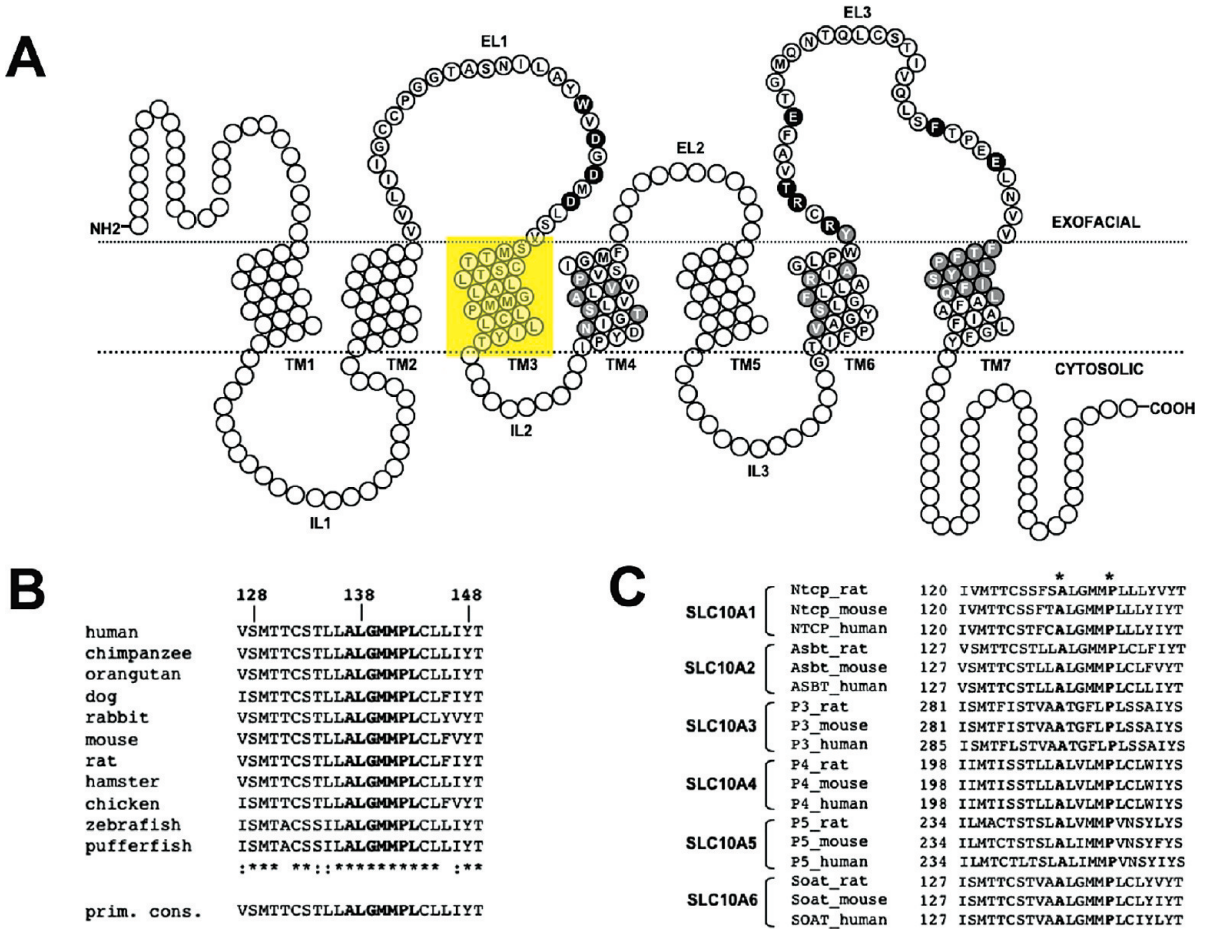

FIGURE 1: TM3 sequence conservation and signature motif. (A) ASBT secondary structural model highlighting regions analyzed via SCAM analysis thus far with amino acid identity of these evaluated regions denoted by their single letter designations. Residues shaded in black putatively either interact directly with sodium ions or bile acid substrates or form crucial contact points mediating substrate-binding events (*15*, *19*). Residues shaded in light gray indicate solvent-accessible sites lining transmembrane helices (*16*−*18*). The yellow rectangle indicates the SCAM target for the present study, specifically residues lining TM3. (B) Sequence alignment of amino acids comprising the TM3 helix (V127−T149) for all known ASBT species. Sequences were retrieved from GenBank and aligned via the MULTALIN routine with annotation performed via MPSA. Asterisks (*) denote complete amino acid conservation among all species, while colons (:) indicate a single conserved amino acid replacement. The ASBT/NTCP/SOAT consensus motif ALGMMPL is denoted by bold lettering (*22*). The bottom line indicates primary consensus for the TM3 region. (C) Sequence alignment for TM3 helices of all SLC10A family members within various species. Asterisks (*) and bold lettering indicate the complete conservation of A127 and P142 among all SLC10A members.

rationale: (i) localization of the SLC10A1/2/6:ASBT/NTCP/SOAT signature motif "ALGMMPL" within TM3 (positions 137−143) (*21*, *22*) and (ii) proximity of the TM3 helix to the large extracellular loop 1 (EL1), previously found to bind sodium and 7α-OH groups on the cholestane skeleton of bile acids (*19*). In particular, the presence of a membrane-bound proline residue (P142) within the TM3 helix, specifically within the ASBT/NTCP/SOAT signature motif, may have important structural or functional implications. Numerous studies have highlighted the role of membranous prolines in helix packing (*23*) and stabilization of α-helical and loop conformations (*24*). Moreover, membranous prolines in bacteriorhodopsin mediate rates of protein folding and assembly (*25*). In membrane transporters and ion channels, functional roles for membranous prolines as cation binding sites (*26*) or molecular switches guiding protein conformational changes (*27*, *28*) have also been reported. Our mutagenesis results demonstrate that P142 may be essential for both ASBT membrane expression and transport activity. Subsequent thiol modification studies of cysteine mutants lining the TM3 helix suggest that solvent accessibility remains unexpectedly confined to the cytosolic half of the helix and can be altered by substrate binding events. On the basis of the significantly decreased substrate affinity of TM3 solvent-accessible mutants, we conclude that the distal half of TM3, comprising residues L145−T149, may form portions of the substrate exit pathway. We also present unique data on select cysteine mutants lining the TM7 helix, which we have previously shown to form portions of the substrate translocation pathway (*17*). Integration of results for TM3 and TM7 cysteine mutants suggests a putative scenario to describe substrate entry and exit into the ASBT permeation pathway during translocation mechanisms.

MATERIALS AND METHODS

Materials. [^{3}H]Taurocholic acid (0.2 Ci/mmol) was purchased from American Radiolabeled Chemicals, Inc. (St. Louis, MO); taurocholic acid (TCA), glycodeoxycholic acid (GDCA), and glycoursodeoxycholic acid (GUDCA) were from Sigma (St. Louis, MO); sulfosuccinimidyl-2-(biotinamido)ethyl-1,3-dithiopropionate (sulfo-NHS-SS-biotin) was from Pierce Chemical Co. (Rockford, IL); [2-(trimethylammonium)ethyl] methanethiosulfonate (MTSET) and 2-((biotinoyl)amino)ethyl methanethiosulfonate (MTSEA-biotin) were from Toronto Research Chemicals, Inc. (North York, Ontario, Canada); biotin ethylenediamine

thiosulfate, sodium salt (TS-biotin), was from Biotium (Hayward, CA). Cell culture media and supplies were obtained from Invitrogen (Rockville, MD). All other reagents and chemicals were of the highest purity available commercially.

Cell Culture and Transient Transfections. COS-1 cells (ATCC CRL-1650) were maintained in Dulbecco's modified Eagle's medium containing 10% fetal calf serum, 4.5 g/L glucose, 100 units/mL penicillin, and 100 μg/mL streptomycin (Life Technologies, Inc., Rockville, MD) at 37 °C in a humidified atmosphere with 5% CO_2. Transient transfections were performed as previously described (*29*).

Site-Directed Mutagenesis. Site-directed mutations were incorporated into C270A-hASBT cDNA using the QuikChange site-directed mutagenesis kit from Stratagene (La Jolla, CA), and mutagenesis primers were custom synthesized and purchased from Sigma Genosys (St. Louis, MO). Plasmid purifications were performed using a kit from Qiagen (Valencia, CA), and amino acid substitutions were confirmed via DNA sequencing using an ABI 3700 DNA analyzer (Applied Biosystems, Foster City, CA) at the Plant-Microbe Genomics Facility of The Ohio State University. Mutant M140C could not be constructed and is absent from the analysis. Residues C132 and C144 are endogenous cysteines and also absent from the analysis.

Uptake Assay and Protein Membrane Expression. Initial rates of transport for each mutant were determined in transiently transfected COS-1 cells incubated in modified Hanks' balanced salt solution (MHBSS), pH 7.4, uptake buffer containing 5.0 μM [^{3}H]TCA at 37 °C for 12 min. This uptake period ensures linear steady-state kinetics in conjunction with an optimal signal-to-noise ratio for subsequent [^{3}H]TCA analysis via liquid scintillation counting (*13*, *17*, *29*). Uptake was halted by a series of washes with ice-cold Dulbecco's phosphate-buffered saline (DPBS), pH 7.4, containing 0.2% fatty acid free bovine serum albumin (BSA) and 0.5 mM TCA. Cells were lysed in 350 μL of 1 N NaOH and subjected to liquid scintillation counting using an LS6500 liquid scintillation counter (Beckmann Coulter, Inc., Fullerton, CA) and total protein quantification using the Bradford protein assay (Bio-Rad, Hercules, CA). Uptake activity was calculated as picomoles of [^{3}H]TCA internalized per minute per milligram of protein. For bile acid uptake kinetics, constants were derived by fitting data to the Michaelis−Menten equation: $V = V_{max}[S]/(K_m + [S])$, where [S] is bile acid concentration, V_{max} is uptake rate at saturating [S], and K_m is substrate concentration at $0.5V_{max}$.

Total and cell surface protein expression was determined via immunoblotting with chemiluminescent detection as described previously (*19*). Blots were probed for positive and negative controls, the plasma membrane marker α-integrin (150 kDa), and the endoplasmic reticulum membrane protein calnexin (90 kDa), respectively, to assess the integrity of the biotinylation procedure (calnexin data not shown). Relative hASBT membrane expression was standardized to integrin expression and quantified via densitometry as previously described (*17*).

Sodium Activation. Measurement of [^{3}H]TCA uptake at equilibrating extracellular Na^+ concentrations (12 mM, i.e., at equilibrium with cytosolic [Na^+]) was performed (uptake conducted as described above; choline chloride used as equimolar NaCl replacement) and expressed as a ratio of uptake at physiological (137 mM) Na^+ concentrations to determine overall sensitivity of each mutant to the presence/absence of Na^+. Mutant ratios are then normalized to C270A for ease of comparison. Theoretically, Na^+ ratios equal to one suggest minimal sensitivity of the transporter to decreased sodium, while fractions less than one indicate a greater necessity for physiological Na^+ concentrations for proper transport function of a mutant transporter.

MTS Inhibition Studies. Thiol accessibility to modification by the positively charged, membrane-impermeant MTSET (1 mM) was determined by preincubation of transiently transfected COS-1 cells for 10 min at room temperature, followed by two washes with modified Hanks' balanced salt solution (Sigma, St. Louis, MO) and [^{3}H]TCA uptake as described above. MTSET solutions were freshly prepared prior to each study due to its short aqueous half-life.

Substrate and Cation Protection Assays. The effects of cotransported bile acids and sodium on MTSET labeling were assayed in transiently transfected COS-1 cells washed twice in 1× PBS, pH 7.4, followed by co-incubation with equal concentrations of MTSET and GDCA (1 mM) prepared either in MHBSS or in Na^+-free buffer (SFB; MHBSS except choline chloride entirely substitutes NaCl) for 10 min at room temperature. After preincubation treatments, cells were washed twice in either MHBSS, pH 7.4, or SFB and additionally equilibrated for 15 min at 37 °C in these buffers followed by determination of [^{3}H]TCA uptake as described above. All control wells were treated identically. MTSET inhibition was determined for each mutant by calculating the ratio of mutant uptake at each experimental condition versus its respective unmodified control. Mutant ratios were then expressed as a percentage of C270A ratio calculated in the same manner.

Labeling of Cysteine Mutants with Biotin-Linked Thiol Derivatives. For studies using the electroneutral reagent MTSEA-biotin, COS-1 cells transiently expressing each mutant were washed twice with either MHBSS, pH 7.4, or SFB followed by incubation with 0.5 mL of MTSEA-biotin (2 mM) prepared in either buffer for 30 min at room temperature with rocking. For studies evaluating the effect of bile acid substrate on biotin labeling, cells were co-incubated with both GDCA (1 mM) and MTSEA-biotin prepared in either MHBSS, pH 7.4, or SFB as described above. For MTSET competition studies, cells were first preincubated with MTSET (1 mM) prepared in SFB for 10 min at room temperature and then washed twice with SFB followed by MTSEA-biotin labeling as described above. For each experiment, a 200 mM stock solution of MTSEA-biotin was prepared in DMSO and kept cold and dark until appropriately diluted with SFB just before use. Biotin labeling was halted by a series a washes with ice-cold PBSCM containing 100 mM glycine, and cells were processed for streptavidin capture and immunoblotting as described previously (*19*). For studies using TS-biotin, intact monolayers of COS-1 cells transiently expressing each mutant were washed twice with MHBSS, pH 7.4, and incubated with 0.5 mL of TS-biotin (2 mM) prepared in MHBSS, pH 7.4, for 30 min at room temperature with rocking. For GDCA protection studies, cells were co-incubated with both GDCA (1 mM) and TS-biotin prepared in MHBSS, pH 7.4, as described above. TS-biotin (2 mM) solutions for each experiment were prepared immediately before use. The biotinylation reaction was halted as described above and processed for immunoblotting as described previously (*19*). All biotinylation studies were repeated on two separate occasions ($n = 2$).

Data Analysis. For each mutant, data are represented as mean ± SD of at least three different experiments with triplicate measurements. Data analysis was performed with GraphPad Prism 4.0 (GraphPad Software, San Diego, CA) using analysis of

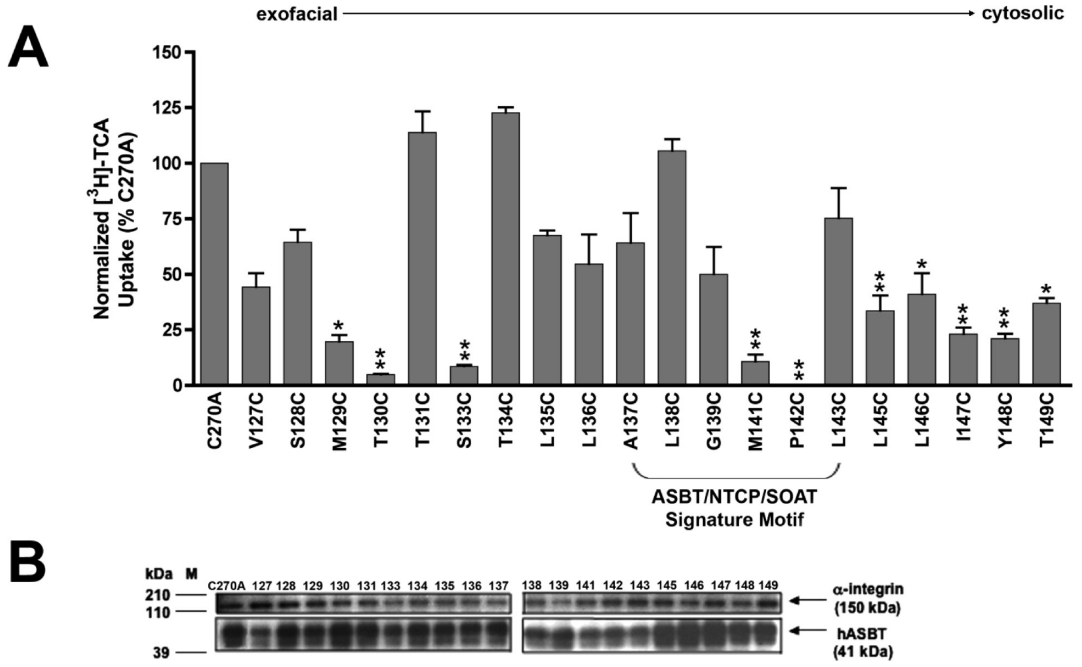

FIGURE 2: [^{3}H]TCA uptake activity and membrane expression of TM3 cysteine mutants. (A) [^{3}H]TCA uptake activity normalized to relative cell surface expression as described in the Materials and Methods section. Bars represent mean ± SD of three separate experiments with $p \leq 0.01$ (**) and 0.05 (*), respectively, using ANOVA with Dunnett's *post hoc* analysis. (B) Intact transfected COS-1 cells were treated with sulfo-NHS-SS-biotin as described in Materials and Methods followed by Western blot processing. Blots were probed with the anti-hASBT antibody (1:15000 dilution) followed by horseradish peroxide-linked anti-rabbit immonuglobin (1:2000 dilution). Each blot was probed for the internal plasma membrane marker, α-integrin (150 kDa), and the absence of calnexin (90 kDa) (data not shown), an endoplasmic reticulum membrane protein representing the negative control in the biotinylated fractions. Marker lanes are shown on the left side of the individual blots. Mature glycosylated hASBT visualizes as the 41 kDa band while the lower, 38 kDa band (not indicated) represents the unglycosylated species.

variance (ANOVA) with Dunnett's *post hoc* test or Student's *t* test as appropriate. Data were considered statistically significant at $p \leq 0.05$.

RESULTS

TM3 Sequence Conservation and Signature Motif. Based on the prevailing 7TM topology, residues V127−T149 (Figure 1A) comprise the TM3 helix. Sequence comparisons suggest a high degree of conservation along this membranous domain (74%) among evolutionarily diverse species (Figure 1B). Particularly interesting is the amino acid string "ALGMMPL" (amino acids 137−143), denoted the ASBT/NTCP/SOAT signature motif (bold letters; Figure 1B), which represents the region of greatest conservation among three key SLC10 members that have quite divergent substrate selectivities (*22*). Whereas ASBT transports strictly bile acids, the liver homologue NTCP exhibits affinity for both bile acids and steroid sulfates (*30*). The recently cloned SOAT lacks bile acid transport affinity and instead transports organic anions and steroid sulfates (*21*, *31*). Thus, it is unlikely that the ASBT/NTCP/SOAT signature motif mediates direct interactions with substrate for these carriers and may instead play indirect roles during the transport cycle. It is also noteworthy that within the signature motif, G139 pairs with P142 in the order GXXP (X = any amino acid), since it has been reported that glycines often pair with membrane-bound prolines using this motif, presumably to mediate Pro-induced structural effects along a helical segment (*32*). Interestingly, P142 remains preserved within various species of remaining SLC10 family members (i.e., SLC10A3-5; Figure 1C), suggesting its putative importance to the overall transport process for carriers in this family. Based on these observations, it is possible that the ASBT/NTCP/SOAT motif within TM3 plays an important structural role during the ASBT transport cycle. Based on protein sequence, the extracellular half of the TM3 helix lies within intimate proximity to functionally important residues D122 and D124 (Figure 1A), which we have previously identified as critical for sodium binding and bile acid interactions, respectively (*19*). These highly conserved aspartic acids are localized to the descending arm of extracellular loop 1 (EL1), which leads into the membrane to form the TM3 helix (Figure 1A). These observations support a role for TM3 during the ASBT transport cycle.

Transport Activity and Membrane Expression of TM3 Mutants. Uptake activity and membrane expression for all cysteine mutants were assayed in transiently transfected COS-1 cells. Surface expression of mutant proteins was measured via biotin labeling with the membrane-impermeant sulfo-NHS-SS-biotin followed by streptavidin capture and immunoblotting with subsequent densitometry of developed protein bands (Figure 2B). For each sample, protein bands corresponding to ASBT were standardized to an internal control (α-integrin) and expressed as a percentage of C270A intensity. Initial uptake activity was then normalized to relative membrane expression for each mutant (Figure 2A).

Replacement of TM3 residues with cysteine, which is relatively hydrophobic and average in bulk, significantly impaired transport activity for half of all mutants assayed (50%; 10 of 20; Figure 2A). Measurable surface expression was detected for all mutants (Figure 2B), suggesting that the severe loss of transport activity (< 10%) for mutants T130C, S133C, M141C, and P142C did not result from lack of protein at the cell surface. Overall, sites exhibiting significantly decreased activity mainly clustered along the helical end segments, closest to the exofacial and cytosolic environments. Moreover, the majority of these activity-impaired

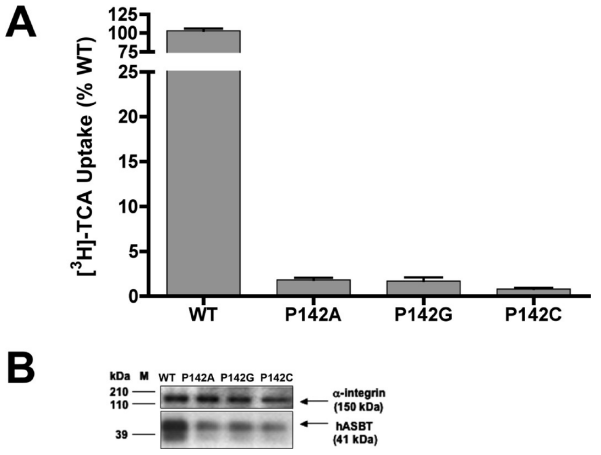

FIGURE 3: [^{3}H]TCA uptake and membrane expression of P142 mutants. Alanine, glycine, and cysteine substitutions of P142 created against the WT background were assayed for (A) normalized initial [^{3}H]TCA uptake and (B) plasma membrane expression as described under Materials and Methods. Bars represent mean ± SD of at least three separate measurements. Data are expressed as a percentage of WT values for each condition. Student's *t* test analysis was performed with activities of all P142 constructs statistically different from WT control at $p < 0.001$ (asterisks omitted for clarity).

mutants were hydrophobic (i.e., M129C, M141C, L143C, L145C, L146C, I147C, Y148C; Figure 2A), with the exception of T130C, S133C, P142C, and T149C. Surprisingly, residues lining the ASBT/NTCP/SOAT signature motif (i.e., A137−L143) were fairly tolerant to replacement, likely a consequence of the relatively conserved nature of cysteine replacement at these positions (Figure 2A). Only two adjacent residues within the motif were severely hampered by mutation, specifically M141 and P142. Compared to other amino acids, prolines are strucutally unique, and their presence may lead to structural distortions and flexibility along α-helical protein segments or induce turns within a β-sheet conformation. If such structural features are critical for protein function, then that particular proline residue will prove highly intolerant to replacement. To test this hypothesis, we generated multiple single mutants of P142 using the native WT protein as the mutagenic template followed by assessment of activity and expression levels (Figure 3). Single mutants P142A, P142C, and P142G were essentially inactive compared to WT, although decreased membrane expression for each mutant was also observed (Figure 3B). These data suggest that impairments in membrane trafficking and insertion occur upon P142 mutation. Normalization of uptake activity to membrane expression did not significantly increase transport activity (Figure 3A), suggesting that P142 mutant constructs expressed at the plasma membrane were functionally impaired. These data indicate that P142 plays an important role to both proper protein expression at the plasma membrane and functional transport activity; moreover, this membranous proline appears intolerant to mutagenesis.

Na^+ Sensitivity of Cysteine Mutants. ASBT concentrates bile acids within the cell interior by coupling movement of one bile acid molecule to the passive flow of at least two sodium ions down their electrochemical gradient (*2*). Our recent studies suggest that two highly conserved negatively charged residues lining EL1 (D122) and EL3 (E261) form the putative sodium sensors during the ASBT transport cycle (*15*, *19*). Studies with ASBT ortho/paralogues corroborate these findings (*33*, *34*). TM3 lies within intimate proximity to the sodium sensor D122 and may therefore play a role during during sodium binding and translocation events. To test this hypothesis, we examined mutant activity at lowered (12 mM) versus physiological (137 mM) extracellular Na^+ concentrations and calculated the ratio of uptake at these two concentrations (12 mM/137 mM). Such a scheme may uncover functional defects consequent to mutation that are otherwise hidden at saturating concentrations of the cotransported sodium ion. Accordingly, our C270A parental template displays minimal alterations in activity at these differing sodium concentrations (*16*, *17*, *19*, *29*), suggesting nominal effects of alanine substitution at the native C270 position.

Although less than half of the TM3 membrane segment exhibited sodium sensitivity (43%; 8 of 17 mutants), these sites intersperse the domain with a distinctly α-helical periodicity, suggesting the presence of discrete faces along the TM3 domain that may be important during sodium binding events. Such a pattern becomes visually evident upon *in silico* rendering of sodium-sensitive sites lining the TM3 helix using our homology model (Figure 4B), wherein two separate helical faces exhibiting sodium sensitivity can be distinguished: one face formed by residues S128, G139, L143, and I147 and the second by residues V127, T134, Leu138, and T149. Interestingly, these helical faces are orientated adjacent to each other in such a manner that they span a rotational axis of approximately 180° around the TM3 α-helical core. These data suggest an "amphipathic" character to TM3 participation during sodium binding and translocation events, in the sense that one-half of the helix may be important for sodium interactions, while the opposite half appears sodium insensitive. These data corroborate a proposed role for TM3 during sodium binding or translocation events.

Solvent Accessibility and Substrate Protection Studies of TM3 Cysteine Mutants. Intact COS-1 monolayers expressing mutant transporters were preincubated with buffer containing 1 mM MTSET followed by several washes before evaluation of remaining [^{3}H]TCA uptake activity. Presumably, only mutants with sulfhydryl groups facing an aqueous milieu (rather than lipid or internal protein environments) will form the more reactive (thiolate) species targeted by MTS reagents for modification (*35*). Surprisingly, most MTSET-inhibited sites, with the exception of S128C, were clustered along the distal end of the TM3 helix closest to the membrane−cytosol juncture (i.e., L143C−T149C; not shown). It is noteworthy that residues lining this distal (or cytosolic) half of TM3 also exhibited transport defects upon mutation (i.e., L145C−T149C; Figure 2). Mutant S128C, which lies at the approximate origin of the TM3 helix as it weaves from the exofacial milieu through the lipid bilayer, represents the only site localized to the exofacial half of the helix amenable to MTSET modification. These data suggest that introduced thiol groups lining predominantly the cytosolic half of TM3 are accessible for modification by the membrane-impermeant MTSET reagent.

Next, protection studies were performed for mutants S128C and L145C−T149C, in which MTSET (1 mM) preincubation was performed in the presence/absence of sodium and/or the natural high-affinity ASBT substrate, glycodeoxycholic acid (GDCA; K_m = 2.0 ± 0.4 mM). Significant protection from MTSET labeling was observed for all accessible sites when MTSET preincubation was performed in the presence of GDCA substrate and/or absence of sodium (Figure 5A). Mutants L143C and T149C constitute the only exceptions; specifically, the concomitant absence of sodium and presence of GDCA

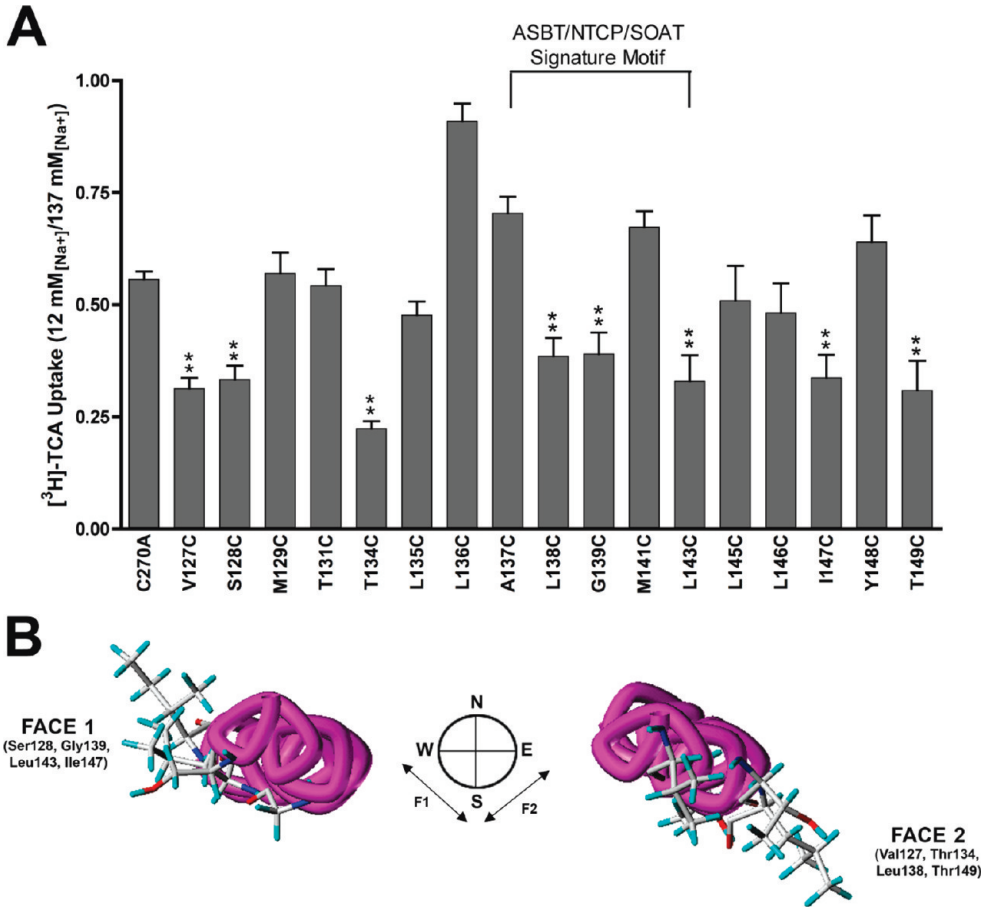

FIGURE 4: Sodium sensitivity of cysteine mutants. (A) COS-1 cells expressing mutant transporters were incubated in uptake medium (5 μM [^{3}H]TCA) containing low (12 mM) or physiological (137 mM) Na^+ concentrations as described under Materials and Methods. Sodium ratios were calculated for each mutant as the quotient of activity at 12 mM versus 137 mM [Na^+]. Bars represent mean activity $\pm$ SD ($n = 3$). Asterisks (**) denote $p \leq 0.01$. (B) Top view of the TM3 helix (i.e., from the exofacial matrix) showing sodium-sensitive residues that comprise two spatially distinct helical faces. These two faces overlap an approximately 180° rotation around the TM3 helical axis.

increased MTSET labeling for mutant L143C, while the absence of sodium exerted no significant protection from MTSET labeling for mutant T149C. Overall, these data suggest that binding of sodium and/or bile acids can modulate MTSET accessibility of TM3 mutants. It should be noted that the TM3 helix contains two endogenous cysteines (C132, C144; Figure 1A) that while essential for function (*29*) cannot be accessed by even 10 mM MTSET concentrations (i.e., 10-fold higher than in present study) (*17*), suggesting orientation of their thiol groups within a lipid or internal protein environment inaccessible to MTS modification. However, the possibility exists that mutagenesis along TM3 may expose these hidden endogenous cysteines to subsequent thiol modification. As mutation at both C132 and C144 abolishes transport activity, creation of a mutagenic scaffold lacking these residues is not experimentally feasible (*29*). Therefore, we propose two scenarios that may account for our data: (i) that TM3 solvent accessibility indeed clusters along the most distal or cytosolic residues or (ii) that endogenous cysteines C132 and/or C144 become exposed upon mutagenesis of adjacent residues and account for the inhibition of activity observed for mutants S128C and L143C−T149C. It should be emphasized that irrespective of the scenario the fact that sodium and bile acids alter MTSET reaction rates indicates that this helical region participates in some manner during the translocation cycle. Furthermore, our data clearly indicate that the TM3 helix contains solvent-accessible pores situated deep within the membrane, irrespective of whether the modification target was introduced thiols or subsequently exposed endogenous cysteines. Finally, based on degree of MTSET inhibition (i.e., MTSET reaction rates), residues L143 and L145 are more solvent accessible than residues closer to the membrane−cytosol juncture (i.e., L146−T149; Figure 5A), at least to the membrane-impermeant and positively charged MTSET reagent.

Labeling of TM3 Cysteine Mutants with Biotin-Linked Thiol Modifiers. Since thiol modification with reagents such as MTSET only examines the functional effects of chemical modification, it is possible that some residues are accessed and modified but do not display any functional consequences. This may be the case for residues lining the exofacial half of TM3 that did not demonstrate any inhibition of activity after 1 mM MTSET pretreatment. In this event, TM3 solvent accessibility would not be confined to the cytosolic half but extend throughout the length of the helix as it traverses the lipid bilayer. To evaluate such a possibility, intact COS-1 monolayers expressing each mutant were incubated with an MTS-biotin derivative, specifically MTSEA-biotin, followed by capture of biotin-labeled proteins with streptavidin. Subsequent immunoblotting permits visualization of the solvent-accessible cysteines introduced along the TM3 helix (Figure 5B). In one set of studies, labeling was done after preincubation with or without MTSET (1 mM) to determine if MTSET and MTSEA-biotin bind the same sites. In another set of studies, labeling was done in the presence and

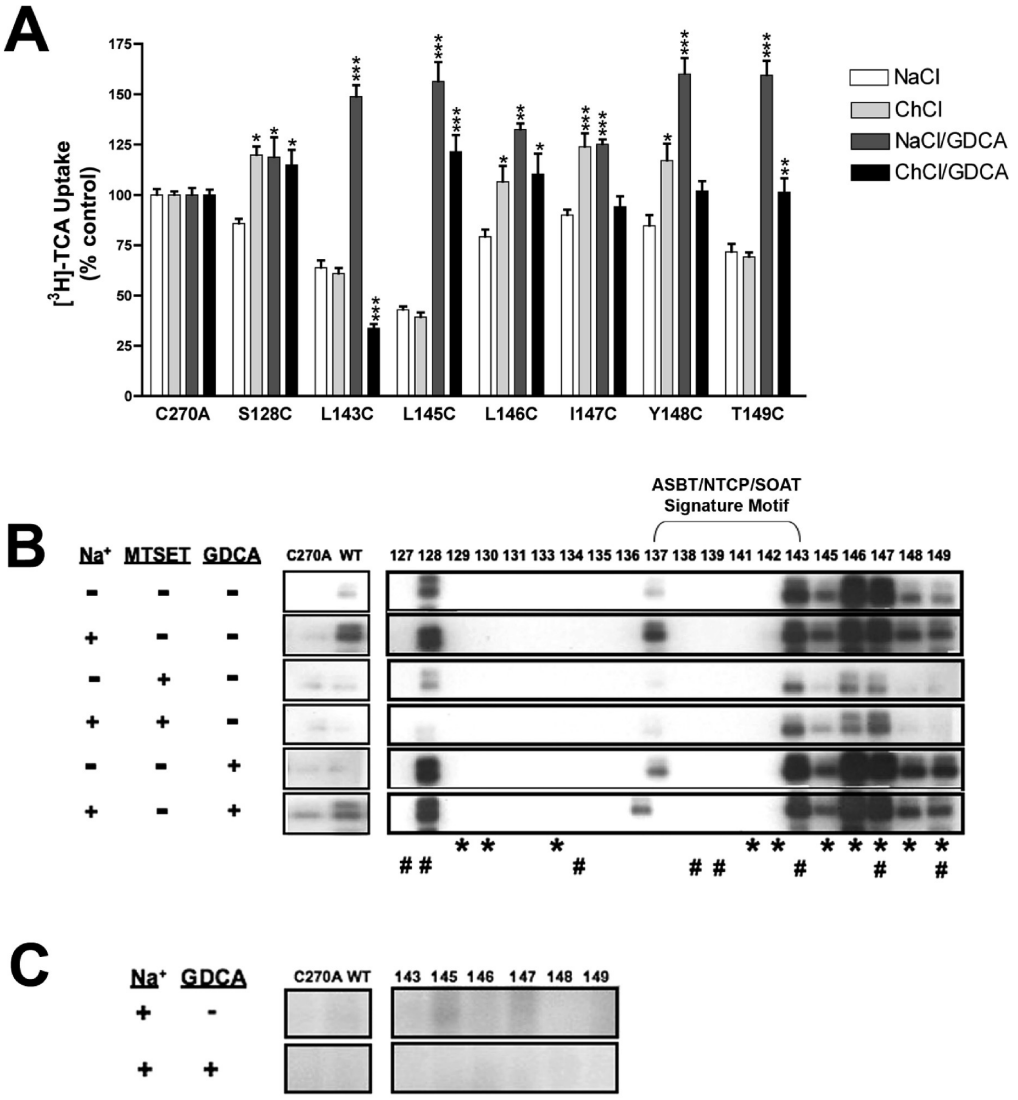

FIGURE 5: TM3 solvent accessibility profile suggests involvement of the cytosolic half of the helix during subtrate translocation. (A) Transiently transfected COS-1 cells were preincubated with 1 mM MTSET prepared in buffer containing either 137 mM NaCl (white bar), 137 mM choline chloride (gray bar), 137 mM NaCl and 1 mM GDCA (dark gray bar), or 137 mM choline chloride and 1 mM GDCA (black bar) and followed by [^{3}H]TCA uptake as described in Materials and Methods. Choline chloride does not activate the transporter and provides equimolar replacement for NaCl. All control wells were treated identically. Bars represent mean ± SD of at least three separate measurements. Data are expressed as a percentage of C270A values for each condition as described under Materials and Methods. Student's *t* test analysis was performed with *, $p < 0.05$, and **, $p < 0.01$. (B) Intact transfected COS-1 cells were treated with MTSEA-biotin (2 mM) in the indicated conditions. For MTSET competition studies, cells were first preincubated with MTSET (1 mM) prepared in buffer with and without sodium for 10 min at room temperature followed by MTSEA-biotin incubation as described in Materials and Methods. For GDCA protection studies, co-incubation of MTSEA-biotin (2 mM) with the bile acid substrate GDCA (1 mM) was performed as described in Materials and Methods. All samples were then submitted to Western blot processing, and blots were probed with the anti-hASBT antibody (1:15000 dilution) followed by horseradish peroxide-linked anti-rabbit immonuglobin (1:2000 dilution). ASBT is detected as two bands, representing the mature glycosylated (41 kDa, top band) and unglycosylated (38 kDa, lower band) species. Negative (C270A) and positive (WT) controls are included to confirm specificity of reaction. Asterisks (*) denote sites with hampered activity upon cysteine mutation, while pound signs (#) signify sodium-sensitive sites. (C) Intact transfected COS-1 cells were treated with TS-biotin (2 mM) in the indicated conditions as described in Materials and Methods. Samples were processed for immunoblotting as described in (B).

absence of GDCA to determine if bile acid substrates could alter labeling. Finally, for all studies, reagents were prepared in both Na^+-free and Na^+-containing buffer to determine the effects of the cotransported sodium ion on labeling efficiency. Both negative (C270A) and positive (WT) controls were included in our measurements to confirm the specificity of biotin labeling. In the native protein, only C270 can be labeled with MTSEA-biotin (*17*) and accounts for the uptake inhibition observed upon thiol labeling with membrane-impermeant MTS reagents (*17*, *29*).

Remarkably, the labeling profile for MTSEA-biotin (Figure 5B) confirms that solvent accessibility of TM3 remains predominantly confined to S128 and the cytosolic half of the helix (L143-T149), as indicated by the pattern of functional inhibition obtained using MTSET (Figure 5A). Mutant A137C constitutes the only exception, as it exhibits MTSEA-biotin labeling in the presence of sodium without corresponding MTSET inhibition of activity. Since pretreatment of L137C with MTSET abolished its MTSEA-biotin labeling, we can conclude that this site is indeed accessed by MTSET, but the consequences are functionally silent. For mutants L143C−T149C, MTSET pretreatment reduces, but does not entirely displace, MTSEA-biotin labeling (Figure 5B). Electrostatic and steric constraints may account for

this differential accessibility, since MTSET and MTSEA-biotin vary in their charge and relative molecular volume. Specifically, MTSET carries a positive charge at physiological pH, while the relatively larger MTSEA-biotin is electroneutral. Next, we sought to determine the effects of bile acids on TM3 solvent accessibility by co-incubating MTSEA-biotin with the high-affinity substrate GDCA (1 mM). Interestingly, GDCA added in the presence of sodium exposes the previously inaccessible L136C while simultaneously blocking biotin labeling at the formerly accessible A137C (Figure 5C), suggesting a conformational change in protein structure along these two sites induced by the simultaneous presence of both cotransported ligands (Na^+, bile acids). Biotin labeling for the remaining sites (S128C, L143C−T149C) was relatively unaltered by GDCA co-incubation.

Since MTSEA-biotin carries no charge, the possibility exists that it may permeate across the lipid bilayer (*36*−*38*), allowing for thiol modification from both the exofacial and cytosolic milieu. Such an occurrence may explain the only partial displacement of MTSEA-biotin labeling by MTSET, since MTSET is membrane-impermeant while MTSEA-biotin could potentially access sites along TM3 from both sides of the lipid membrane. Thus, we next examined accessibility of the cytosolic half of TM3 (L143−T149) to a positively charged biotin-linked thiol derivative, TS-biotin, which is membrane-impermeant. Our results demonstrate that sites L143C−T149C, which are highly accessible to biotin labeling with MTSEA-biotin, cannot be accessed by the membrane-impermeant TS-biotin, suggesting limited accessibility of these cytosolic residues from the exofacial milieu (Figure 5C). These results also confirm that MTSEA-biotin likely accesses the hydrophilic cleft along the cytosolic half of TM3 from both the exofacial and cytosolic milieu, accounting for the increased labeling rate observed with MTSEA-biotin versus MTSET and TS-biotin. Minimal changes in accessibility were detected when TS-biotin incubation was performed in the presence of bile acid substrate GDCA. Size constraints may account for accessibility of L143C−T149C to modification by the electropositive MTSET (1 mM; Figure 5A) but not to biotin labeling with the similarly charged TS-biotin (Figure 5C). Since MTSET is approximately half the size of TS-biotin (278.24 vs 462.54 g/mol), it could potentially access aqueous cavities with smaller molecular volumes or situated deeper into the lipid bilayer compared to TS-biotin. Finally, although ASBT contains endogenous cysteines located within cytosolic protein regions, our controls (Figure 5B, C) ensure that introduced, rather than endogenous, cysteines are responsible for the labeling of distal TM3 sites. Overall, our results strongly suggest the presence of a large hydrophilic pore or cavity predominantly lining the cytosolic half of the TM3 helix that exhibits limited solvent accessibility from the extracellular matrix but appears highly accessible from the cytosolic milieu.

Labeling of TM7 Cysteine Mutants with Biotin-Linked Thiol Modifiers. In an earlier study, we reported the presence of a large hydrophilic cavity lining the exofacial half of TM7 using functional inhibition screening of cysteine mutants with various physicochemically different MTS reagents (MTSES, MTSET, MTSEA) (*17*). In the present study, we screened TM7 cysteine mutants lining this large hydrophilic cavity (F287C−Q297C) for their accessibility to biotin labeling with both MTSEA-biotin and TS-biotin, which was not performed in our earlier scan. These studies were intended as a comparative control for our TM3 solvent accessibility data, since our earlier study concluded that TM7 lines portions of the substrate permeation pathway. Our results with both biotin-linked thiol modifiers (i.e., MTSEA-biotin, TS-biotin) confirm the high degree of solvent accessibility along the exofacial half of TM7 in the presence of sodium (Figure 6A). More interestingly, we report changes in accessibility along this TM7 cavity in the presence of bile acid substrates, suggesting conformational sensitivity of this hydrophilic cleft region to thiol labeling. Specifically, preincubation of TM7 mutants with MTSEA-biotin in the presence of GDCA (1 mM) increases biotin labeling of all sites except F289, Y293, and S294, which instead exhibit decreased labeling (Figure 6A). When MTSEA-biotin preincubation was performed in the presence of glycoursodeoxycholic acid (GUDCA; K_m = 11.5 ± 2.0 μM), a bile acid varying in hydroxylation pattern and affinity, the biotin labeling profile was similar to that obtained with GDCA, except for sites F287 and F289 (Figure 6A). Moreover, relatively increased biotin labeling was observed for I295C using preincubation with GUDCA versus GDCA. Thus, our data suggest that bile acids induce conformational changes along the TM7 helix that may promote their binding. Interestingly, these results also imply that bile acid structure potentially influences the nature of these local conformational changes. However, additional studies using a panel of structurally diverse bile acids are needed to make definitive conclusions. Finally, MTSET pretreatment before MTSEA-biotin application completely abrogated biotin labeling, suggesting that MTSET and MTSEA-biotin bind the same sites along the TM7 helix.

Preincubation of TM7 mutants with the membrane-impermeant TS-biotin in the presence of sodium (Figure 6B) further confirms the presence of a large hydrophilic cavity along the extracellular half of TM7 that can be easily accessed from the exofocial mileu. Interestingly, labeling with the electropositive TS-biotin also demonstrates conformational sensitivity to the presence of bile acid substrate (GDCA). Specifically, all mutants except I292C, Y293C, and F296C exhibited marked differences in biotin labeling rates in the presence of GDCA (Figure 6B). Since MTSEA-biotin and TS-biotin are relatively similar in size (381.52 vs 462.54 g/mol), it is likely that the relative polarity of each reagent accounts for differences in biotinylation rates at specific sites along the TM7 cleft region.

Uptake Kinetics of Select TM3 and TM7 Cysteine Mutants. To further establish the role of residues lining putative hydrophilic cleft regions along the exofacial half of TM7 and the cytosolic half of TM3, we submitted select cysteine mutants to kinetic evaluation. TM3 mutants S128C and L145C−T149C and TM7 mutants F287C, F289C, L291C, and Y293C were submitted to kinetic analyses based on (i) their significantly decreased initial TCA transport activity upon cysteine mutation (Figure 2) (*17*) and (ii) high degree of solvent accessibility as determined using both functional (i.e., MTSET) and visual (i.e., TS/MTSEA-biotin) thiol modifiers (Figures 5 and 6) (*17*). TCA kinetic constants for C270A, WT, and mutant transporters assayed in transiently transfected COS-1 monolayers were then generated via nonlinear least-squares fitting procedures (Table 1). TCA affinities (μM) for C270A (7.9 ± 1.95) and WT (11.6 ± 2.39) ASBT protein agree with previously published values from our laboratory and are not significantly different, confirming their kinetic similarity. In contrast, TCA affinity was significantly decreased for all mutants assayed except for Y148C and T149C (Table 1). These data implicate participation of residues S128 and L145−I147 in TM3 and residues F287, F289, L291, and Y293 in TM7 during bile acid recognition, binding, and translocation events. Coupled to results from our solvent accessibility studies, these data corroborate putative roles

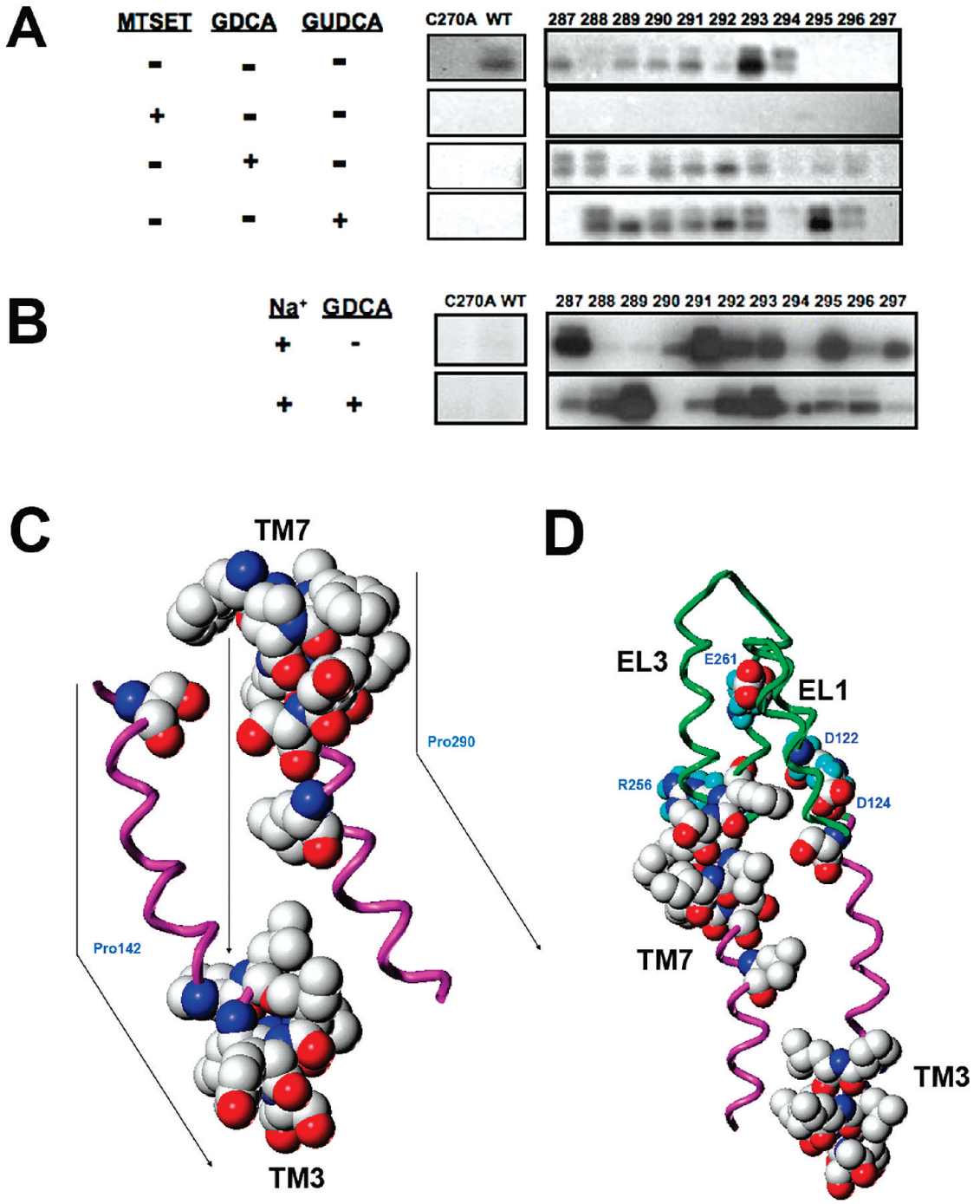

FIGURE 6: The exofacial half of TM7 forms the substrate entrance route during permeation events. (A) Intact transfected COS-1 cells were treated with MTSEA-biotin (2 mM) in the indicated conditions as described in Materials and Methods and processed for immunoblotting to visualize the solvent accessibility of the large hydrophilic cavity lining the exofacial half of TM7, spanning residues F287−Q297 (*17*). Preincubation with MTSET (1 mM) confirms that MTSEA-biotin and MTSET bind the same sites along TM7, while co-incubation with the native bile acids GDCA and GUDCA (1 mM) suggests that bile acid substrates induce conformational changes in local structure along the TM7 exofacial cleft region. (B) Solvent accessibility profile of TM7 mutants to TS-biotin labeling as described in Materials and Methods. (C) *In silico* rendering of the relative orientation of TM7 and TM3 solvent-accessible cavities with putative P142- and P290-induced distortions of helices indicated by arrows. The putative translocation "pathway" formed between TM7 and TM3 is also indicated. Space-filled format used to depict amino acids. (D) TM7 and TM3 hydrophilic cavities depicted in relation to putative substrate (D124, R256) and sodium (D122, E261) interaction sites lining EL1 and EL3 protein regions (*15*, *19*). Hydrogen atoms on amino acids omitted for visual clarity.

for residues lining these hydrophilic exofacial and cytosolic cleft regions during substrate translocation events.

DISCUSSION

The present study examines solvent accessibility of consecutively introduced cysteines along transmembrane helix 3 (V127−T149) of ASBT. Our key findings include (i) the functional and structural importance of P142, located within the ASBT/NTCP/SOAT signature motif, during the ASBT transport cycle, (ii) identification of a large hydrophilic cleft region lining the most distal or cytosolic half of the TM3 helix, and (iii) development of a model positing the contribution of the hydrophilic cleft regions lining TM3 and TM7 during substrate

Table 1: TCA Kinetic Constants for C270A, WT, TM3, and TM7 Cysteine Mutants[a]

	taurocholate kinetics	
construct	K_t (μM)	J_{max} (pmol min^{-1} (mg of protein)$^{-1}$)
C270A	7.9 ± 1.95	655.6 ± 32.46
WT	11.6 ± 2.39	176.3 ± 7.08
S128C	17.24 ± 4.74	309.9 ± 20.7
L145C	16.51 ± 3.77	281.2 ± 15.47
L146C	15.56 ± 3.52	1223 ± 65.60
I147C	22.72 ± 4.93	1454 ± 82.81
F287C	61.52 ± 5.86	1016 ± 32.77
F289C	34.44 ± 7.37	302.3 ± 18.49
L291C	35.44 ± 6.32	1047 ± 53.77
Y293C	72.03 ± 20.83	1364 ± 72.00

[a]COS-1 cells transiently transfected as described in Materials and Methods. Uptake measured at TCA concentrations ranging from 0 to 150 μM (measured in triplicate). Kinetic data analyzed using Graphpad Prism software with constants determined via nonlinear least-squares fitting procedures. Bile acid affinity (K_m) for all mutant constructs significantly different from controls, $p < 0.05$. Asterisks omitted for visual clarity.

translocation. These conclusions are derived from data generated by site-directed mutagenesis, thiol modification studies, and computational analysis using our previously developed homology model (*14*).

After normalization to protein surface expression, half of all TM3 cysteine mutants exhibited significant decreases in transport activity (Figure 3), suggesting a functional role for this helical segment during the ASBT transport cycle. Interestingly, mutagenesis of only two residues within the ASBT/NTCP/SOAT signature motif (ALGMMPL; amino acid positions 137−143) resulted in impaired transport activity, specifically at M141 and P142. These data suggest that despite its high degree of conservation, amino acid substitution along portions of the signature motif can be functionally tolerated. However, additional conservative (Gly) and nonconservative (Ala, Cys) mutagenesis of P142 suggests that this membranous proline along TM3 is essential for function, since activity of these constructs remains severely (< 5%) hampered, even after normalization to protein cell surface expression. Intriguingly, a recent Pro-scanning mutagenesis study of glycophorin A (GpA) demonstrated that replacement of membranous prolines located within the helix center abolished helix packing (*39*). P142 lies close to the helix midpoint, and it is tempting to speculate a role for it in modulating TM3 helix packing within the lipid bilayer. In turn, TM3 packing within the lipid bilayer may be functionally essential for ASBT transport activity in general. Additionally, numerous studies with transport proteins and ion channels have implicated membranous prolines in forming biomolecular switches that allow the regulated, reversible conformational changes in protein structure requisite for substrate translocation across the lipid bilayer (*23*, *26*, *28*, *32*, *40*−*44*). Within the SLC10 family, P142 has been entirely preserved (Figure 1C), suggesting its importance to transporter activity irrespective of the cargo transferred across the lipid membrane. Our mutagenesis data support the functionally essential nature of P142, although, at present, it is difficult to define its exact role during the transport cycle. We have previously reported a similarly essential proline residue within the TM6 helix, which in conjunction with two functionally essential glycines modulates the conformational flexibility of TM6 during substrate permeation (*16*).

Studies in which extracellular sodium levels were decreased highlight a putative role for TM3 residues during sodium interaction and permeation events. Potentially, mutants that exhibit hampered activity at low (12 mM) versus saturating (137 mM) sodium concentrations may be situated within or around sodium interaction sites or form secondary contacts necessary for proper protein structure during sodium binding. Such an approach was used to identify a stripe of critical amino acid residues lining TM7 of the serotonin transporter, which the authors suggest are important in sodium binding or coupling of binding events to later translocation steps in the transport cycle (*45*). Based on the periodicity of mutants exhibiting hampered uptake activity at low versus saturating sodium concentrations, the TM3 helix contains two distinct sodium sensitive faces. *In silico* rendering of these hampered sites using our homology model visually corroborates the spatial separation of these sodium-sensitive mutants along two separate and adjacent helical faces. These results suggest that approximately half of the TM3 helix has some role during sodium binding and permeation events (Figure 4). Since one of the putative sodium sensors, D122 (*15*), is situated only four amino acids removed from the origin (or relative beginning) of the TM3 helical segment (Figure 1A), it is tempting to speculate that sodium binding at this site is somehow "sensed" or otherwise transduced along these TM3 residues. For instance, binding of sodium may cause conformational changes in local protein structure that facilitate downstream events leading to substrate turnover; sodium-sensitive residues within TM3 may contribute to this process. Alternatively, some of these residues may be involved in mediating sodium permeation, since a number of these sites are polar in nature and could provide surfaces for cation interactions (i.e., S128, T134, T149).

Site-directed alkylation studies of TM3 cysteine mutants indicate the presence of a large hydrophilic cleft region predominantly lining the cytosolic half of the TM3 helix. Inhibition studies using the positively charged, membrane-impermeant MTSET identified only residues S128 and L143−T149 as solvent accessible. While S128 lies close to the membrane−exofacial juncture, residues L143−T149 are situated at the very distal end of the TM3 helix closest to the cell cytosol. Substrate protection studies suggest that these MTSET-accessible sites are conformationally sensitive to sodium and/or bile acid binding, since rates of MTSET modification could be significantly decreased when sodium or bile acid was added/removed to the preincubation medium. Substrate protection from MTSET modification may result from two scenarios: (i) occlusion of these sites from labeling due to local changes in protein structure upon bile acid or sodium binding or (ii) physical blockage of these sites by bile acids or sodium during binding or translocation events. Kinetic analysis of these mutants (Table 1) reveals that sites S128 and L145−I147 are important for bile acid substrate interactions, since TCA affinity is significantly lower for these constructs versus control. Overall, these data suggest a role for the cytosolic half of TM3 during bile acid substrate translocation events. Next, we used MTSEA-biotin to determine whether any TM3 cysteine mutants were solvent accessible, but without any functional consequence. Strikingly, the MTSEA-biotin labeling profile essentially mirrors MTSET solvent accessibility: only mutants S128C and L143C−T149C are biotin labeled (with the exception of L136C and A137C; Figure 5B). These data confirm that solvent accessibility along

TM3 remains confined to the cytosolic half, while the rest of the helix remains situated within the lipid bilayer or internal protein environments.

Based on the degree of MTSET displacement of the MTSEA-biotin signal (Figure 5A), the cytosolic TM3 cavity is more accessible to MTSEA-biotin labeling than to MTSET. Since this hydrophilic cavity extends deeply into the membrane, electrostatic constraints may hamper the positively charged MTSET from accessing sites that are readily available to the electroneutral MTSEA-biotin. The MTSET inhibition profile itself reflects such a scenario, since the degree (or severity) of uptake inhibition decreases for sites deeper into the cavity. For example, the two most severely inhibited residues (L143C, L145C; Figure 6A) lie at the approximate "beginning" of the cavity, while deeper into the membrane, relatively less MTSET inhibition is observed. On the other hand, MTSEA-biotin may be also accessing these residues from the cytosol, which would explain why GDCA alters MTSET modification rates (Figure 6A) but minimally affects MTSEA-biotin labeling. To further test this assumption, we investigated whether the cytosolic cleft region along TM3 could be accessed by the positively charged, membrane-impermeant TS-biotin reagent. Our results demonstrate that minimal biotin labeling of these sites occurs using a thiol modifier similar in size to MTSEA-biotin that cannot penetrate into or through the lipid bilayer (Figure 5C). These results strongly suggest that the hydrophilic cleft region lining the cytosolic half of TM3 exhibits limited solvent accessibility from the exofacial milieu but remains highly accessible from the cytosolic milieu. Moreover, the limited access attainable from the exofacial matrix may be guided by steric and charge restrictions.

Our previous study implicated the exofacial half of TM7 (Figure 1A) in bile acid translocation (*17*). In the present report, biotin labeling with MTSEA/TS-biotin corroborates the high degree of solvent accessibility along this exofacial cavity. Moreover, substrate protection studies offer striking evidence of the conformational sensitivity of these residues to sodium and bile acid binding events (Figure 6). We have previously shown conformational sensitivity of extracellular loop 1 (EL1) to MTSEA-biotin, particularly along the distal or descending portions of the loop leading into the TM3 helix. Incubation with bile acid substrates and/or removal of sodium blocked access to cysteine mutants spanning the latter half of EL1. Results from the present study further corroborate that large-scale global changes in protein structure occur during the ASBT transport cycle. Kinetic analysis of TM7 mutants F287C, F289C, L291C, and Y293C demonstrate significantly decreased TCA affinity, suggesting that these sites are involved during bile acid substrate recognition and permeation events. Based on the accumulated data thus far, it is likely that conformational sensitivity at these TM7 sites results from the physical presence of bile acid substrate blocking thiol labeling.

Integrating results of the current study with our previous analyses, we propose the following hypothetical model (Figure 6C): (i) that the exofacial half of TM7 forms portions of an initial entry point for bile acid substrates present in the extracellular mileu and may participate during substrate entry into the protein core and (ii) that the cytosolic half of TM3 may form portions of the substrate permeation pathway during later stages of substrate translocation, for instance, during substrate release into the cell interior. Thus, the relatively small MTSET may travel along the permeation path provided by the hydrophilic cleft along TM7 to gain limited access to distal TM3 sites, while the electroneutral MTSEA-biotin accesses the TM3 cavity from both the exofacial and cytosolic milieu. On the other hand, the charged and bulky TS-biotin cannot access TM3 distal sites either from the exofacial or cytosolic milieu. Interestingly, both TM helices contain functionally critical helix-distorting proline residues (P142, P290) (Figure 3) (*46*), which may play a role in helical flexibility important for the translocation process. Presently, further studies are required to make definitive conclusions regarding the role of these prolines during substrate permeation. It should be noted that, at this stage of investigation, our model remains an approximation of ASBT transport mechanisms, based on investigational approaches that have inherent caveats that should be taken into consideration. Mutagenic analysis, while highly successful and ubiquitous to protein structure−function analysis, constitutes an alteration to the native protein and, potentially, to the native conformational states. Thus, the possibility exists that solvent accessibility profiles for the native protein may vary to some extent from those observed using the C270A mutagenic construct. Moreover, we interpret our data using our previously developed homology model, which remains simply a model that may deviate to some degree from the actual three-dimensional structure of the protein in the physiological setting. Additionally, our model posits specific roles for only two membrane spanning segments, TM3 and TM7, during substrate translocation mechanisms. Other protein regions are likely involved in this process and contribute to the overall transport cycle. Indeed, additional mechanisms that have yet to be investigated may be occurring in conjunction with the roles proposed for TM3 and TM7, such as the possibility of reentrant loops. Such a mechanism was posited for the liver bile acid transporter NTCP based on membrane-insertion scanning (*47*) and remains to be experimentally investigated for ASBT.

In conclusion, we report the functional and structural significance of the membranous P142 residue, localized within the ASBT/NTCP/SOAT signature motif during ASBT substrate turnover. Moreover, the cytosolic half of TM3 may form a putative substrate exit route, which in conjunction with the TM7 substrate entrance route lining the exofocial half of the helix may provide a mechanistic model detailing key steps of the ASBT transport cycle.

REFERENCES

1. Pauli-Magnus, C., Stieger, B., Meier, Y., Kullak-Ublick, G. A., and Meier, P. J. (2005) Enterohepatic transport of bile salts and genetics of cholestasis. *J. Hepatol. 43*, 342–357.
2. Weinman, S. A., Carruth, M. W., and Dawson, P. A. (1998) Bile acid uptake via the human apical sodium-bile acid cotransporter is electrogenic. *J. Biol. Chem. 273*, 34691–34695.
3. Trauner, M., and Boyer, J. L. (2003) Bile salt transporters: molecular characterization, function, and regulation. *Physiol. Rev. 83*, 633–671.
4. Huang, H. C., Tremont, S. J., Lee, L. F., Keller, B. T., Carpenter, A. J., Wang, C. C., Banerjee, S. C., Both, S. R., Fletcher, T., Garland, D. J., Huang, W., Jones, C., Koeller, K. J., Kolodziej, S. A., Li, J., Manning, R. E., Mahoney, M. W., Miller, R. E., Mischke, D. A., Rath, N. P., Reinhard, E. J., Tollefson, M. B., Vernier, W. F., Wagner, G. M., Rapp, S. R., Beaudry, J., Glenn, K., Regina, K., Schuh, J. R., Smith, M. E., Trivedi, J. S., and Reitz, D. B. (2005) Discovery of potent, nonsystemic apical sodium-codependent bile acid transporter inhibitors (Part 2). *J. Med. Chem. 48*, 5853–5868.
5. Huff, M. W., Telford, D. E., Edwards, J. Y., Burnett, J. R., Barrett, P. H., Rapp, S. R., Napawan, N., and Keller, B. T. (2002) Inhibition of the apical sodium-dependent bile acid transporter reduces LDL cholesterol and apoB by enhanced plasma clearance of LDL apoB. *Arterioscler. Thromb. Vasc. Biol. 22*, 1884–1891.
6. Izzat, N. N., Deshazer, M. E., and Loose-Mitchell, D. S. (2000) New molecular targets for cholesterol-lowering therapy. *J. Pharmacol. Exp. Ther. 293*, 315–320.

7. Kitayama, K., Nakai, D., Kono, K., van der Hoop, A. G., Kurata, H., de Wit, E. C., Cohen, L. H., Inaba, T., and Kohama, T. (2006) Novel non-systemic inhibitor of ileal apical Na^+-dependent bile acid transporter reduces serum cholesterol levels in hamsters and monkeys. *Eur. J. Pharmacol. 539*, 89–98.
8. Li, H., Xu, G., Shang, Q., Pan, L., Shefer, S., Batta, A. K., Bollineni, J., Tint, G. S., Keller, B. T., and Salen, G. (2004) Inhibition of ileal bile acid transport lowers plasma cholesterol levels by inactivating hepatic farnesoid X receptor and stimulating cholesterol 7 alpha-hydroxylase. *Metabolism 53*, 927–932.
9. West, K. L., McGrane, M., Odom, D., Keller, B., and Fernandez, M. L. (2005) SC-435, an ileal apical sodium-codependent bile acid transporter inhibitor alters mRNA levels and enzyme activities of selected genes involved in hepatic cholesterol and lipoprotein metabolism in guinea pigs. *J. Nutr. Biochem. 16*, 722–728.
10. West, K. L., Ramjiganesh, T., Roy, S., Keller, B. T., and Fernandez, M. L. (2002) 1-[4-[4-[(4*R*,5*R*)-3,3-Dibutyl-7-(dimethylamino)-2,3,4,5-tetrahydro-4-hydroxy-1,1-dioxido-1-benzothiepin-5-yl]phenoxy]butyl]-4-aza-1-azoniabicyclo[2.2.2]octane methanesulfonate (SC-435), an ileal apical sodium-codependent bile acid transporter inhibitor alters hepatic cholesterol metabolism and lowers plasma low-density lipoprotein-cholesterol concentrations in guinea pigs. *J. Pharmacol. Exp. Ther. 303*, 293–299.
11. Balakrishnan, A., and Polli, J. E. (2006) Apical sodium dependent bile acid transporter (ASBT, SLC10A2): a potential prodrug target. *Mol. Pharmaceutics 3*, 223–230.
12. Balakrishnan, A., Wring, S. A., and Polli, J. E. (2006) Interaction of native bile acids with human apical sodium-dependent bile acid transporter (hASBT): influence of steroidal hydroxylation pattern and C-24 conjugation. *Pharm. Res. 23*, 1451–1459.
13. Banerjee, A., and Swaan, P. W. (2006) Membrane topology of human ASBT (SLC10A2) determined by dual label epitope insertion scanning mutagenesis. New evidence for seven transmembrane domains. *Biochemistry 45*, 943–953.
14. Zhang, E. Y., Phelps, M. A., Banerjee, A., Khantwal, C. M., Chang, C., Helsper, F., and Swaan, P. W. (2004) Topology scanning and putative three-dimensional structure of the extracellular binding domains of the apical sodium-dependent bile acid transporter (SLC10A2). *Biochemistry 43*, 11380–11392.
15. Banerjee, A., Hussainzada, N., Khandelwal, A., and Swaan, P. W. (2008) Electrostatic and potential cation-pi forces may guide the interaction of extracellular loop III with Na^+ and bile acids for human apical Na^+-dependent bile acid transporter. *Biochem. J. 410*, 391–400.
16. Hussainzada, N., Khandewal, A., and Swaan, P. W. (2008) Conformational flexibility of helix VI is essential for substrate permeation of the human apical sodium-dependent bile acid transporter. *Mol. Pharmacol. 73*, 305–313.
17. Hussainzada, N., Banerjee, A., and Swaan, P. W. (2006) Transmembrane domain VII of the human apical sodium-dependent bile acid transporter ASBT (SLC10A2) lines the substrate translocation pathway. *Mol. Pharmacol. 70*, 1565–1574.
18. Khantwal, C. M., and Swaan, P. W. (2008) Cytosolic half of transmembrane domain IV of the human bile acid transporter hASBT (SLC10A2) forms part of the substrate translocation pathway. *Biochemistry 47*, 3606–3614.
19. Hussainzada, N., Claro da Silva, T., Zhang, E. Y., and Swaan, P. W. (2008) Conserved aspartic acid residues lining extracellular loop I of sodium-coupled bile acid transporter ASBT interact with Na^+ and 7alpha-OH moieties on the ligand cholestane skeleton. *J. Biol. Chem.* (in press).
20. Kaback, H. R., Dunten, R., Frillingos, S., Venkatesan, P., Kwaw, I., Zhang, W., and Ermolova, N. (2007) Site-directed alkylation and the alternating access model for LacY. *Proc. Natl. Acad. Sci. U.S.A. 104*, 491–494.
21. Geyer, J., Godoy, J. R., and Petzinger, E. (2004) Identification of a sodium-dependent organic anion transporter from rat adrenal gland. *Biochem. Biophys. Res. Commun. 316*, 300–306.
22. Geyer, J., Wilke, T., and Petzinger, E. (2006) The solute carrier family SLC10: more than a family of bile acid transporters regarding function and phylogenetic relationships. *Naunyn-Schmiedeberg's Arch. Pharmacol. 372*, 413–431.
23. Woolfson, D. N., and Williams, D. H. (1990) The influence of proline residues on alpha-helical structure. *FEBS Lett. 277*, 185–188.
24. Shelden, M. C., Loughlin, P., Tierney, M. L., and Howitt, S. M. (2001) Proline residues in two tightly coupled helices of the sulphate transporter, SHST1, are important for sulphate transport. *Biochem. J. 356*, 589–594.
25. Lu, H., Marti, T., and Booth, P. J. (2001) Proline residues in transmembrane alpha helices affect the folding of bacteriorhodopsin. *J. Mol. Biol. 308*, 437–446.
26. Sansom, M. S. (1992) Proline residues in transmembrane helices of channel and transport proteins: a molecular modelling study. *Protein Eng. 5*, 53–60.
27. Brandl, C. J., and Deber, C. M. (1986) Hypothesis about the function of membrane-buried proline residues in transport proteins. *Proc. Natl. Acad. Sci. U.S.A. 83*, 917–921.
28. Sansom, M. S., and Weinstein, H. (2000) Hinges, swivels and switches: the role of prolines in signalling via transmembrane alpha-helices. *Trends Pharmacol. Sci. 21*, 445–451.
29. Banerjee, A., Ray, A., Chang, C., and Swaan, P. W. (2005) Site-directed mutagenesis and use of bile acid-MTS conjugates to probe the role of cysteines in the human apical sodium-dependent bile acid transporter (SLC10A2). *Biochemistry 44*, 8908–8917.
30. Hagenbuch, B., and Meier, P. J. (1996) Sinusoidal (basolateral) bile salt uptake systems of hepatocytes. *Semin. Liver Dis. 16*, 129–136.
31. Geyer, J., Doring, B., Meerkamp, K., Ugele, B., Bakhiya, N., Fernandes, C. F., Godoy, J. R., Glatt, H., and Petzinger, E. (2007) Cloning and functional characterization of human sodium-dependent organic anion transporter (SLC10A6). *J. Biol. Chem. 282*, 19728–19741.
32. Cordes, F. S., Bright, J. N., and Sansom, M. S. (2002) Proline-induced distortions of transmembrane helices. *J. Mol. Biol. 323*, 951–960.
33. Sun, A. Q., Balasubramaniyan, N., Chen, H., Shahid, M., and Suchy, F. J. (2006) Identification of functionally relevant residues of the rat ileal apical sodium-dependent bile acid cotransporter. *J. Biol. Chem. 281*, 16410–16418.
34. Zahner, D., Eckhardt, U., and Petzinger, E. (2003) Transport of taurocholate by mutants of negatively charged amino acids, cysteines, and threonines of the rat liver sodium-dependent taurocholate cotransporting polypeptide Ntcp. *Eur. J. Biochem./FEBS 270*, 1117–1127.
35. Karlin, A., and Akabas, M. H. (1998) Substituted-cysteine accessibility method. *Methods Enzymol. 293*, 123–145.
36. Chen, J. G., Liu-Chen, S., and Rudnick, G. (1998) Determination of external loop topology in the serotonin transporter by site-directed chemical labeling. *J. Biol. Chem. 273*, 12675–12681.
37. Chen, R., Wei, H., Hill, E. R., Chen, L., Jiang, L., Han, D. D., and Gu, H. H. (2007) Direct evidence that two cysteines in the dopamine transporter form a disulfide bond. *Mol. Cell. Biochem. 298*, 41–48.
38. Seal, R. P., Leighton, B. H., and Amara, S. G. (2000) A model for the topology of excitatory amino acid transporters determined by the extracellular accessibility of substituted cysteines. *Neuron 25*, 695–706.
39. Orzaez, M., Salgado, J., Gimenez-Giner, A., Perez-Paya, E., and Mingarro, I. (2004) Influence of proline residues in transmembrane helix packing. *J. Mol. Biol. 335*, 631–640.
40. Hirai, T., and Subramaniam, S. (2003) Structural insights into the mechanism of proton pumping by bacteriorhodopsin. *FEBS Lett. 545*, 2–8.
41. Bright, J. N., Shrivastava, I. H., Cordes, F. S., and Sansom, M. S. (2002) Conformational dynamics of helix S6 from Shaker potassium channel: simulation studies. *Biopolymers 64*, 303–313.
42. Joshi, A. D., and Pajor, A. M. (2006) Role of conserved prolines in the structure and function of the Na^+/dicarboxylate cotransporter 1, NaDC1. *Biochemistry 45*, 4231–4239.
43. Slepkov, E. R., Chow, S., Lemieux, M. J., and Fliegel, L. (2004) Proline residues in transmembrane segment IV are critical for activity, expression and targeting of the Na^+/H^+ exchanger isoform 1. *Biochem. J. 379*, 31–38.
44. Tieleman, D. P., Shrivastava, I. H., Ulmschneider, M. R., and Sansom, M. S. (2001) Proline-induced hinges in transmembrane helices: possible roles in ion channel gating. *Proteins 44*, 63–72.
45. Penado, K. M., Rudnick, G., and Stephan, M. M. (1998) Critical amino acid residues in transmembrane span 7 of the serotonin transporter identified by random mutagenesis. *J. Biol. Chem. 273*, 28098–28106.
46. Wong, M. H., Oelkers, P., and Dawson, P. A. (1995) Identification of a mutation in the ileal sodium-dependent bile acid transporter gene that abolishes transport activity. *J. Biol. Chem. 270*, 27228–27234.
47. Mareninova, O., Shin, J. M., Vagin, O., Turdikulova, S., Hallen, S., and Sachs, G. (2005) Topography of the membrane domain of the liver Na^+-dependent bile acid transporter. *Biochemistry 44*, 13702–13712.